Food Chemistry: X 22 (2024) 101448

Contents lists available at ScienceDirect

Food Chemistry: X

journal homepage: www.sciencedirect.com/journal/food-chemistry-x

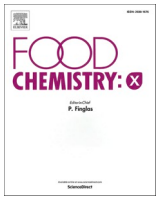

Effects of different protein cross-linking degrees on physicochemical and subsequent thermal gelling properties of silver carp myofibrillar proteins sol subjected to freeze-thaw cycles

Yuxin Ding [a], Ruonan Feng [a], Zhifei Zhu [b,c], Junmin Xu [b,c], Yanshun Xu [a,*]

[a] School of Food Science and Technology, Jiangnan University, 1800 Lihu Ave, Wuxi, Jiangsu 214122, China
[b] Mekong Fishery Industry Co.,Ltd, Veun Kham Village, Don Khong, Champassak, Laos
[c] Shenzhen CF Marine Technology Co., Ltd., 140 Jinye Ave, Shenzhen, Guangdong, 518116 China

ARTICLE INFO

Keywords:
Myofibrillar proteins
Cross-linking
Freeze-thaw cycles
Sol
Gelling properties

ABSTRACT

Knowledge regarding the denaturation process and control methods for depolymerized sol-state myofibrillar proteins (MPs) during freezing remains scant. This study investigated the effects of protein cross-linking treatment before freezing on physicochemical and subsequent gelation properties of MPs sol subjected to freeze-thaw (F-T) cycles. Results indicated that after five F-T cycles, cross-linked MPs sols showed increased high molecular weight polymers and bound water (T_{21a} and T_{21b}) mobility, suggesting enhanced protein-protein interactions at the expense of protein-water interactions. Upon heating after F-T cycles, gels formed from cross-linked sols exhibited significantly higher hardness, springiness, and cooking loss ($P < 0.05$), alongside more contracted gel networks. Correlation analysis revealed that the formation and properties of thermal gel after freezing closely relate to changes in molecular conformation and chemical bonds of cross-linked MPs sol during freezing. This study provides new insights into regulating the freezing stability and post-thawed thermal processing properties of sol-based surimi products.

1. Introduction

Fish-Hua, a Chinese-style fish paste, is a dense blend of salt-soluble proteins derived from the salt-mediated dissociation and expansion of MPs in fish muscle during the mincing process. Distinct from heat-induced surimi gels, surimi sol-based products represented by Fish-Hua preserve their uncooked state (Du et al., 2023). These unique surimi products enjoy widespread popularity, particularly in Asia, due to their rich protein content, minimal fat, and desirable sensory qualities such as elasticity and tenderness (Zhang et al., 2024). Freezing serves as an effective strategy to prevent food spoilage caused by enzymatic and microbial activity, and is widely utilized in the preservation and transport of surimi-based products (Wang et al., 2021). Nonetheless, recurrent temperature changes during freezing can induce several detrimental alterations like ice crystal formation, protein and lipid oxidation, and the disruption of natural structure and functionality of MPs, adversely impacting the consumable quality of the products, including issues like drip loss, altered texture, and dehydration (Tian, Walayat, Ding, & Liu, 2021).

Exogenous transglutaminase (TGase) can improve the freezing quality of MPs gel by catalyzing cross-linking through the reaction between glutamine and lysine in MPs (Yang et al., 2020). Chen et al. (2024) demonstrated that TGase enhanced gelation of MPs in frozen *Litopenaeus vannamei* by promoting cross-linking through deamidation reactions. An, You, Xiong, and Yin (2018) clarified that TGase improved the gelation properties of short-term (5–7 days) frozen surimi by unfolding proteins and exposing reactive groups during initial freezing, thus increasing cross-linking and hydrophobic interactions. Luo et al. (2024) reported that appropriately increasing the degree of cross-linking under various freezing methods made surimi gel structures more robust and stable, inhibiting quality degradation during freezing. However, excessive TGase-induced cross-links can prevent the formation of a uniform protein network, leading to a transition from viscoelastic to brittle in surimi gel (Fang et al., 2021). Thus, regulating the degree of protein cross-linking is crucial for controlling frozen surimi gel quality. However, existing research on protein cross-linking in surimi gel with thermally denatured three-dimensional networks cannot fully explain its role in the freezing process of MPs sol without heat denatured.

* Corresponding author.
E-mail address: xuys@jiangnan.edu.cn (Y. Xu).

https://doi.org/10.1016/j.fochx.2024.101448
Received 15 March 2024; Received in revised form 22 April 2024; Accepted 5 May 2024
Available online 7 May 2024

Surimi sol transitions to a semi-gel at 4 °C, which then gels through protein cross-linking upon heating. Compared to heated gels, sols exhibit weaker protein stretching and cross-linking, resulting in less stable networks during freezing (Liu, Zhang, Xue, & Xue, 2019). The impact of protein cross-linking before freezing on the quality of frozen surimi sol products remains uncertain. Our prior work has shown that the molecular state of MPs before freezing can influence their structural and functional properties during freezing (Feng, Li, Liu, Xia, & Xu, 2022). Consequently, this research elucidated the impacts of protein cross-linking states and molecular structural changes before freezing on the physicochemical properties of MPs sols during F-T cycles and the gel structure changes after freezing, offering valuable insights for quality control of frozen surimi products.

MPs sols with varying cross-linking degrees were prepared by MTGase. The establishment of different cross-linked states of MPs molecules during F-T cycles was verified through the analysis of protein cross-linking degree and sodium dodecyl sulfate-polyacrylamide gel electrophoresis (SDS-PAGE). The moisture distribution and heat-induced gel properties of MPs sols with different levels of protein cross-linking after F-T cycles were evaluated using low field nuclear magnetic resonance (LF-NMR), dynamic rheology, cooking loss, textural properties, and microstructure. The impacts of protein cross-linking on the structural changes and aggregation of sol-state MPs were assessed by examining protein secondary structure, chemical forces, aggregate surface morphology, and sol microstructure. This study aims to investigate the effects of protein cross-linking on MPs sols before and after F-T cycles and its influence on subsequent heat-induced gelation, providing theoretical guidance for the processing and storage of surimi sol or semi-gel products.

2. Materials and methods

2.1. Materials

Silver carp (2.5–3.0 kg each) were purchased from a Wuxi market, Jiangsu, China, and transported alive in water containers to the lab. They were euthanized via stunning, and dorsal muscles were collected and minced for analysis. MTGase (1000 U/g) was purchased from Jiangsu Yiming Biological Co., ltd. (Jiangsu, China). Analytical grade reagents were used throughout.

2.2. Extraction of myofibrillar proteins (MPs)

MPs were extracted from silver carp using a reported method (Yang et al., 2021), involving three washes of the muscle in ice water, 2 min each, followed by rapid chopping with a meat grinder (SUPOR JR05D-300, Supor Co., ltd., Zhejiang, China) for 2 min with each time of 1 min and an interval of 30 s. The ground muscle was homogenized with four volumes of ice-cold 20 mmol/L Tris-HCl buffer (pH 7.2) at 1000 rpm for 5 min, then centrifuged at 13,130*g*, 4 °C for 10 min with a 4 K15 refrigerated centrifuge (Sigma Co., ltd., Germany). The supernatant was discarded, and after three homogenization-centrifugation cycles, the MPs pellet was stored at 4 °C for use within 24 h. Protein concentration was measured using the Coomassie Brilliant Blue method.

2.3. Construction of MPs sol cross-linking system

MPs concentration was set to 60 mg/mL using 20 mmol/L Tris-HCl (pH 7.2) with 2.5% (*w/v*) NaCl. Different cross-linking degrees in MPs sols were achieved by adding MTGase at 0, 0.05, 0.10, 0.15, and 0.20 U/g. Samples were evaluated before freezing (FT 0) and after five freeze-thaw cycles (FT 5), each consisting of freezing at −20 °C for 24 h and thawing at 4 °C for 12 h.

Protein cross-linking degree was measured using the ortho-phthalaldehyde (OPA) method to determine free amino group content. For this, 2 g sol was mixed with 18 mL borax buffer (0.07 mol/L SDS, 0.002 mol/L $Na_2B_4O_7{\cdot}10\ H_2O$, pH 8.9), heated at 75 °C for 15 min to stop proteolysis, then stirred at 60 °C for 2 h for protein extraction. After centrifugation at 10,700 *g* for 20 min, the supernatant was diluted 4× with 1% (*w/v*) SDS. A 200 μL sample of this dilution was combined with 4 mL OPA reagent and incubated for 2 min at room temperature. Absorbance was read at 340 nm, using L-leucine for standard curves and 1% SDS as the blank. The cross-linking degree calculation formula was as follows:

$$\textit{Crosslinking degree}\ (\%) = \left(1 - \frac{a^{'}}{a}\right) \times 100 \tag{1}$$

where a is the free amino group content in the blank group; $a^{'}$ is the free amino group content in the experimental group.

2.4. Protein patterns

The protein profiles of MPs were analyzed using SDS-PAGE. A 2 g sample of MPs sol was blended with 18 mL of 5% (*w/v*) SDS and homogenized for 2 min. The mixture was heated at 85 °C for 1 h, then centrifuged at 10,700 *g* for 20 min. The supernatant was diluted to 3 mg/mL with 5% SDS. For electrophoresis, 150 μL of this solution was mixed with 50 μL of sample loading buffer (4×, 0.2 mol/L Tris-HCl, 0.3 mol/L SDS, 0.006 mol/L bromophenol blue, 200 mL/L glycerin, pH 6.8) and 8 μL of β-mercaptoethanol, boiled for 5 min, and 8 μL loaded onto a 4% stacking gel, then separated on a 10% resolving gel. Staining was done with Coomassie Brilliant Blue R250 and destained until a clear background was obtained, with images captured on a ChemiDoc XRS+ system (Bio-Rad, Hercules, CA, USA).

2.5. Water distribution analysis

Water distribution in MPs sol was analyzed using a LF-NMR analyzer (MesoMR23–060 V-I, Niumag Analytical Instrument Co., Ltd., Suzhou, China) following the previous method (Cao et al., 2022). A 1.5 g sample in a 5 mL tube was examined using a Carr-Purcell-Meiboom-Gill sequence at 21 MHz and 32 °C. Parameters included a 4000 ms interval, 8 scans, 5000 echoes, and 100 kHz frequency. Data was processed with MultiExp Inv software to identify peak times and area proportions.

2.6. Preparation and analysis of heat-induced MPs gel

2.6.1. Preparation of heat-induced MPs gel

MPs sols samples (60 mg/mL), with and without five F-T cycles and different cross-linking degrees, were placed in 50 mL tubes and centrifuged at 430 *g* for 3 min to remove air bubbles. They were then incubated at 40 °C for 30 min, followed by 90 °C for 30 min, and stored at 4 °C for 12 h before analysis.

2.6.2. Dynamic rheological measurement

The rheological properties of MPs sol before and after F-T cycles with different cross-linking degrees were measured following the previous method (Liu et al., 2019), using a DHR-3 rotational rheometer (TA Instruments, USA) with a 40 mm parallel plate. The linear viscoelastic region was identified via strain scanning at 25 °C within 0.1–0.5% strain. Storage (G') and loss (G") modulus were recorded at 1 Hz and 0.5% strain, with temperature ramping from 25 °C to 90 °C at a rate of 5 °C/min.

2.6.3. Cooking loss analysis

Cooking loss was assessed with a minor modification according to the previous method (Fan, Peng, Pang, Wen, & Yi, 2021). The initial weight of MPs sol was noted as M_1, and the post-cooking weight of the heat-induced MPs gel as M_2. Cooking loss was calculated using the formula:

$$Cooking\ loss\ (\%) = \frac{M_1 - M_2}{M_1} \times 100 \quad (2)$$

2.6.4. Texture profile analysis

The hardness and springiness of heat-induced MPs gel were measured through a TA-XT Plus texture analyzer (Stable Micro Systems ltd, Godalming, UK) with a P/36R probe, following the method of Feng et al. (2022). The settings were: a test speed of 1 mm/s, a strain of 50%, and a trigger force of 5 g.

2.6.5. Gel microstructure analysis

The microstructure of heat-induced MPs gel was analyzed using a Scanning Electron Microscope (SEM). Gel slices around 2–3 mm thick were freeze-dried for 48 h in a vacuum freeze dryer (Alpha 1–2 LD plus, Martin Christ Co., Ltd., Germany). After fixing with conductive adhesive, the samples were gold-sputter-coated for imaging. Images were captured at 3.0 kV acceleration voltage and 1000× magnification.

2.7. Analysis of protein structure and aggregation morphology of MPs sol

2.7.1. Secondary structure analysis

A Fourier Transform Infrared (FT-IR) spectrometer (IS10, Nicolet Instruments, USA) was used to assess the protein secondary structures in MPs sol. After freeze-drying, sample powder was blended with potassium bromide at a 1:50 (*w*/w) ratio, ground, and pressed into pellets. Spectra were obtained from 4000 to 400 cm^{-1}, averaging 64 scans at a 4 cm^{-1} resolution. The amide bands in the 1600–1700 cm^{-1} range were deconvoluted through curve fitting with second-derivative peak-splitting in PeakFit software (v4.12) to reduce residuals. This allowed the quantification of α-helices, β-sheets, β-turns, and random coils based on the subpeak areas.

2.7.2. Chemical bonds analysis

Chemical bond analysis in MPs sol was referred to the method of Du et al. (2023). A 2 g sample was mixed with five different solvents: 10 mL each of 0.05 mol/L NaCl (S1), 0.6 mol/L NaCl (S2), 0.6 mol/L NaCl with 1.5 mol/L urea (S3), 0.6 mol/L NaCl with 8 mol/L urea (S4), and 0.6 mol/L NaCl with 8 mol/L urea plus 0.5 mol/L β-Mercaptoethanol (S5). After centrifugation at 12,840 *g* for 15 min at 4 °C, the supernatants were analyzed for protein content. The bonds were categorized as follows: nonspecific bonds = S1, ionic bonds = S2-S1, hydrogen bonds = S3-S2, hydrophobic interactions = S4-S3, and disulfide bonds = S5-S4.

2.7.3. Protein surface morphology analysis

Protein surface morphology was analyzed using an Atomic Force Microscopy (AFM) (Dimension FastScan, Bruker Co., Ltd., Germany) with a TAP 150 probe, following the method described by Wei, Monahan, Zhang, Wang, and Zhang (2023). A 20 μL droplet of 20 μg/mL MPs solution was deposited on a 10 mm × 10 mm polished silicon wafer and dried at room temperature. To eliminate buffer salt effects on imaging, the protein layers were washed five times with distilled water and air-dried. The scanning covered a 5 μm × 5 μm area with a 256 × 256 pixels resolution. The obtained AFM images were processed with NanoScope Analysis 1.7 software, and the average protein height and root mean square roughness (Rq) were calculated.

2.7.4. Sol microstructure analysis

The microstructure of MPs sol was visualized using paraffin embedding, as detailed by Pereira et al. (2021). The sol was fixed in 4% (*w*/*v*) paraformaldehyde (4 °C, 48 h), dehydrated through ethanol and xylene grades, and paraffin-embedded. Microtome sections (10 μm) were placed on slides and oven-dried at 70 °C for 2 h. After xylene dewaxing, sections were stained with hematoxylin-eosin (HE) and imaged at 100× magnification using an upright microscope (EOS600D, Canon, Japan).

2.8. Statistical analysis

Experiments were conducted in triplicate, and data were analyzed using SPSS version 26.0, presented as mean ± standard deviation (SD). Significant differences between means were identified using Duncan's multiple range test, with $P < 0.05$ denoting statistical significance. Correlations between variables were evaluated through a correlation matrix. Graphs were created using Origin 2019 (OriginLab Inc., Northampton, MA, USA).

3. Results and discussion

3.1. Myofibrillar proteins cross-linking

In this study, the cross-linking degrees of MTGase-treated MPs sols were estimated by the quantitative determination of free amino groups (Jia, Huang, & Xiong, 2016), as shown in Table S1. For unfrozen samples, no detectable cross-linking degrees were observed in MPs sols treated with 0.05–0.10 U/g MTGase. However, the significant increases in cross-linking were noted at concentrations of 0.15 U/g and 0.20 U/g MTGase ($P < 0.05$). Chen et al. (2024) have reported that MTGase might facilitate the acyl transfer reactions between the γ-carboxyamide groups of glutamine residues and ε-amino groups of lysine residues, promoting ε-(γ-glutamyl)-lysine isopeptide bond formation and protein cross-linking. Following F-T cycles, cross-linking was evident in all MTGase-treated samples, intensifying with higher MTGase concentrations. Notably, the cross-linking degree in MPs sol with 0.20 U/g MTGase more than doubled after F-T cycles, indicating enhanced cross-linking activity during F-T cycles. This might be because freeze-induced protein unfolding and the exposure of more reactive sites facilitated the cross-linking reactions catalyzed by MTGase.

3.2. Protein pattern

Surimi MPs primarily consist of myosin heavy chain (MHC), actin, and tropomyosin (TM). The distinct protein patterns in MPs sols containing MTGase were shown in Fig. 1. In unfrozen samples, increased MTGase concentrations resulted in more accumulation of protein residues at the stacking gel top (Fig. 1 (a)), suggesting MTGase-catalyzed cross-linking formed high-molecular-weight polymers, varying with MTGase concentrations. The MHC band intensity decreased with higher MTGase, whereas actin and TM bands remained unchanged (Fig. 1 (a)), highlighting MHC as the primary target for MTGase cross-linking. This aligns with Liang et al. (2020), showing MHC as more prone to MTGase-induced cross-linking than actin, possibly due to the lack of reactive lysine residues in actin for MTGase action (Fang et al., 2021). Remarkably, after F-T cycles, MTGase presence intensified the residue accumulation at the stacking gel top and further reduced MHC intensity (Fig. 1 (b)), attributed to protein denaturation and structural extension during F-T cycles, facilitating MTGase-mediated aggregate formation.

3.3. Water distribution and gel properties of MPs sol

3.3.1. Water distribution

LF-NMR analysis provided insights into the mobility and distribution of water molecules in MTGase-treated MPs sols. Fig. S1 shows the distributions of relaxation times (T_2) across MPs sols with varying cross-linking degrees, before and after F-T cycles. T_{21a} (< 1 ms) and T_{21b} (1–10 ms) peaks represent bound water, tightly associated with macromolecules through strong hydrogen bonding (Huang et al., 2019). The T_{22} peak (10–300 ms) corresponds to immobile water within actin, tropomyosin filament and myosin filament. The absence of free water suggested that high ionic strength stabilized water molecules via ionic interactions during the salt-mediated dissociation and expansion of MPs (Shao et al., 2016). Table 1 displays the changes in T_2 relaxation time of MPs sols subjected to different cross-linking treatments before and after

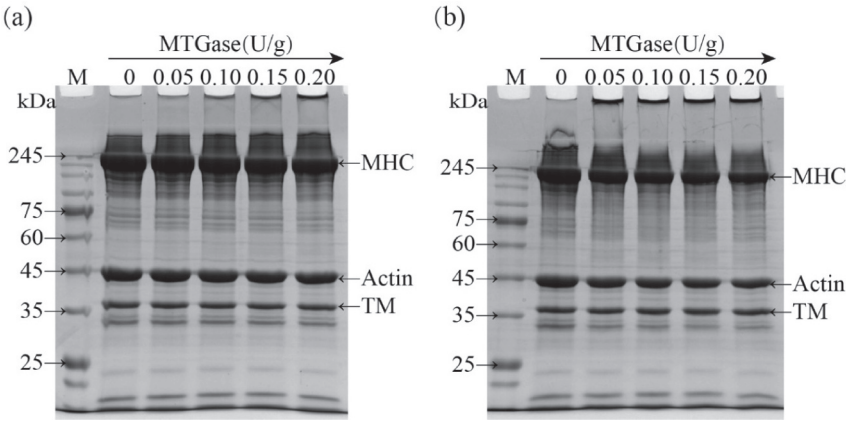

Fig. 1. SDS-PAGE patterns of myofibrillar proteins (MPs) sols with different MTGase concentrations before (a) and after (b) freeze-thaw cycles.

Table 1
Effects of MTGase on T_2 relaxation times of unfrozen (FT 0) and freeze-thawed (FT 5) myofibrillar proteins (MPs) sols.

	MTGase (U/g)	T_{21a}(ms)	T_{21b}(ms)	T_{22}(ms)
FT 0	0	0.55 ± 0.22^{ab}	3.68 ± 0.51^{cd}	155.22 ± 0.10^{b}
	0.05	0.55 ± 0.08^{ab}	4.05 ± 0.72^{c}	155.22 ± 0.10^{b}
	0.10	0.59 ± 0.09^{a}	3.03 ± 0.72^{d}	144.81 ± 0.00^{c}
	0.15	0.54 ± 0.06^{ab}	3.45 ± 0.60^{cd}	144.81 ± 0.00^{c}
	0.20	0.45 ± 0.04^{ab}	3.50 ± 0.38^{cd}	144.81 ± 0.00^{c}
FT 5	0	0.29 ± 0.01^{b}	3.72 ± 0.42^{cd}	166.38 ± 0.00^{a}
	0.05	0.40 ± 0.21^{ab}	4.40 ± 0.17^{c}	166.38 ± 0.00^{a}
	0.10	0.34 ± 0.05^{ab}	5.55 ± 0.39^{b}	166.38 ± 0.00^{a}
	0.15	0.42 ± 0.15^{ab}	6.08 ± 0.25^{b}	166.38 ± 0.00^{a}
	0.20	0.60 ± 0.14^{a}	7.72 ± 0.54^{a}	166.38 ± 0.00^{a}

Data are presented as mean ± SD ($n = 3$). Mean values in the same row with different.
Letters were significantly different ($P < 0.05$).

F-T cycles. In unfrozen sols, MTGase did not significantly alter T_{21a} relaxation times ($P > 0.05$), due to the minimal presence and strong association of bound water with MPs. However, as the MTGase concentration increased from 0 to 0.05 U/g to 0.10–0.20 U/g, the T_{22} time decreased from 155.22 ms to 144.81 ms ($P < 0.05$), indicating restricted mobility of immobile water in MPs sols, consistent with the findings of Luo et al. (2024). After five F-T cycles, T_{21b} and T_{22} times increased in all MPs sols, suggesting that water molecules increased mobility and easily migrated to the extracellular region, leading to ice crystals formation and structural deterioration (Cao et al., 2018). Nakazawa and Okazaki (2020) also found that network damage and protein denaturation might enhance water movement. Furthermore, moisture signal intensity declined with higher MTGase levels during F-T cycles, and T_{21a} and T_{21b} times became more dispersed, indicating a reduced water retention capacity of MPs sols, potentially due to MTGase disrupting protein-water interactions (Zhang et al., 2021).

3.3.2. Dynamic rheological properties

The thermal gelation of MPs sols was effectively analyzed using a temperature sweep, as shown in Fig. 2. Between 25 and 90 °C, the storage modulus (G') remained higher than the loss modulus (G"), indicating the formation of an elastic gel dependent on temperature (Liu, Yang, Chi, & Chi, 2023). In unfrozen samples, two G' increases before 45 °C were attributed to myosin head aggregation after heating (Chen et al., 2022). A significant decrease in G' between 45 °C and 55 °C might result from endogenous proteolytic enzyme activity causing gel matrix collapse (Feng et al., 2022). MTGase application mitigated this G' decline, suggesting that MTGase-induced cross-linking reduced protease-catalyzed hydrolysis and gel matrix weakening (Singh, Prabowo, Benjakul, Pranoto, & Chantakun, 2020). After 55 °C, G' values rose continuously with increasing temperature, further enhanced by higher MTGase concentrations, indicating that heat and MTGase synergistically promoting protein unfolding and reactive sites exposure, facilitating gel network formation through covalent and non-covalent interactions. G" followed a similar pattern (Fig. 2b) but gradually decreased from about 70 °C, indicating a residual viscous nature in the gel matrix (Zhou, Liu, Kang, Cui, & Yang, 2021). As presented in Fig.2c and 2d, after F-T cycles, G' and G" values were notably lower than in unfrozen samples, reflecting weakened gel strength. However, MTGase-catalyzed covalent cross-linking between glutamine and amino groups might counteract the viscoelasticity decline. Specifically, the G' at 90 °C in the uncross-linked sample decreased by 18.37% after freezing, whereas the 0.2 U/g MTGase cross-linked sample decreased by only 1.65%. Thus, MPs sols treated with protein cross-links were more likely to form heat-induced gels with greater viscoelasticity after frozen storage.

3.3.3. Cooking loss, hardness and springiness

Cooking loss (CL) is critical for evaluating the water-holding capacity of gel products. Table 2 shows that the lowest CL occurred in the gel from unfrozen sol without MTGase, and the CL significantly increased as the concentration of MTGase rose. This suggests that the interactions between proteins were enhanced compared to those between water and proteins, lending to water release during heating after F-T cycles. Jia et al. (2016) observed a similar increase in CL with MTGase in black carp protein gels. Combined with the rheological analysis results, it can be inferred that although MTGase-induced cross-linking between γ-carboxyamide and amino groups enhanced MPs sol viscoelasticity, it hindered the uniform formation of gel network, thereby reducing the space for water retention (Guo et al., 2019). F-T cycles could form irregular ice crystals, damaging muscle tissues and denaturing proteins, further reducing the water-holding capacity of MPs gel (Zhang, Cao, Wei, & Ying, 2020). Notably, the 0.20 U/g MTGase sample showed a CL roughly 8.03 times higher than the control, indicating an increase in protein-protein interactions at the expense of water-protein interactions during heating after F-T cycles, leading to gel contraction and water expulsion (Liu, Zhao, Xie, & Xiong, 2011).

Hardness and springiness are essential indicators for gel quality assessment. Table 2 reveals that gels formed from cross-linked MPs sols exhibited significantly enhanced hardness and springiness compared to uncross-linked samples ($P < 0.05$), corroborating the rheological findings. This suggests that MTGase-mediated cross-linking facilitated tail-to-tail interactions among myosin molecules, with the concurrent stretching of proteins during heating contributing to the formation of strong gel matrix. After F-T cycles, MTGase significantly improved the textural attributes (hardness and springiness) of gels compromised by freezing, possibly by enhancing covalent cross-linking and protein polymerization within the sols (Chen et al., 2024).

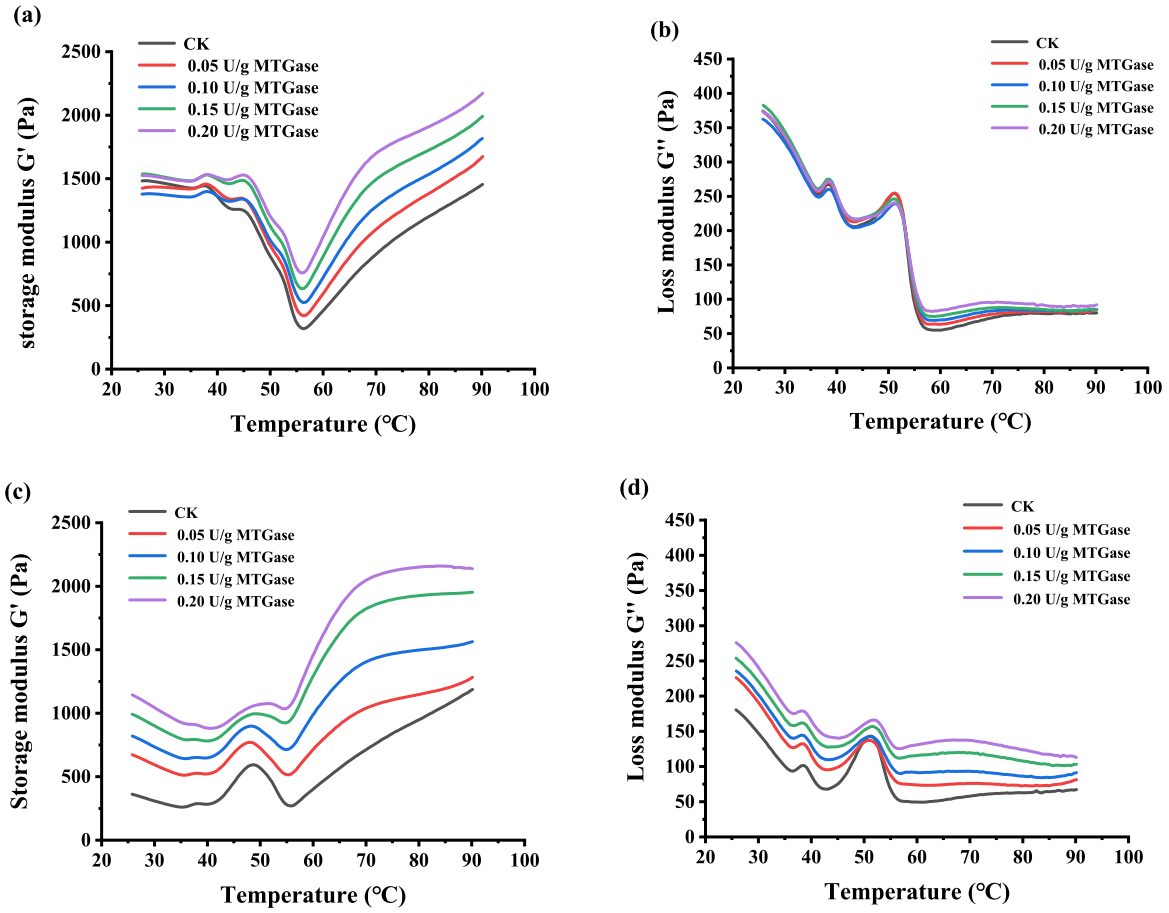

Fig. 2. Effects of MTGase on viscoelastic properties of unfrozen (a, b) and freeze-thawed (c, d) myofibrillar proteins (MPs) sols.

Table 2
Effects of MTGase on cooking loss, hardness and springiness of gels prepared from unfrozen (FT 0) and freeze-thawed (FT 5) myofibrillar proteins (MPs) sols.

	MTGase (U/g)	Cooking loss (%)	Hardness (g)	Springiness (%)
FT 0	0	3.04 ± 0.13^{e}	843.51 ± 18.19^{e}	93.73 ± 0.18^{f}
	0.05	5.22 ± 0.21^{e}	965.71 ± 13.71^{d}	94.36 ± 0.06^{e}
	0.10	11.91 ± 0.08^{d}	1044.51 ± 15.51^{d}	95.49 ± 0.22^{cd}
	0.15	17.72 ± 2.33^{c}	1194.33 ± 86.72^{c}	96.10 ± 0.08^{b}
	0.20	23.25 ± 0.78^{b}	1259.90 ± 68.83^{bc}	96.50 ± 0.18^{a}
FT 5	0	3.38 ± 0.35^{e}	613.61 ± 29.88^{f}	93.17 ± 0.17^{g}
	0.05	6.20 ± 0.52^{e}	1019.14 ± 15.51^{d}	94.51 ± 0.20^{e}
	0.10	13.96 ± 0.11^{d}	1253.31 ± 8.16^{bc}	95.29 ± 0.18^{d}
	0.15	23.56 ± 3.34^{b}	1301.81 ± 38.94^{b}	95.41 ± 0.13^{cd}
	0.20	27.13 ± 1.41^{a}	1428.82 ± 18.28^{a}	95.66 ± 0.19^{c}

Data are presented as mean ± SD (n = 3). Mean values in the same column with different.
Letters were significantly different ($P < 0.05$).

3.3.4. Gel microstructure

As displayed in Fig. 3, the microstructure of heat-induced gel from MPs sol was strongly associated with the CL and textural properties. The unfrozen control displayed a well-ordered three-dimensional network with uniformly small pores and a dense surface. However, MTGase promoted the formation of inter- and intra-molecular non-disulfide covalent bonds between glutamate and lysine residues in MPs gel, leading to the formation of large protein aggregates and expanded pores. This resulted in a looser network, which decreased water retention while increasing gel strength (Section 3.3.3). After F-T cycles, the gel structure was damaged by irregular ice crystals, resulting in a coarse and fragmented gel network (Tang et al., 2019). MTGase helped merge protein structures in frozen sols, forming more stacked and contracted gel networks due to the presence of protein connections and bridges already formed by freezing, which was associated with increased gel hardness, springiness and cooking losses (Chen et al., 2024). Sakamoto et al. (2010) observed similar effects, noting that ε-(γ-Glu)-Lys cross-links could also partially hinder the uniform development of protein network.

3.4. Protein structure and aggregation morphology of MPs sol

3.4.1. Secondary structure

FT-IR spectra of MPs sols, varying in MTGase concentrations and F-T treatments, are presented in Fig. S2, showing consistent spectral patterns across conditions. Typically, the amide I region (1700–1600 cm^{-1}) reflects protein secondary structures (Table 3) (Priyadarshini, Xavier, Nayak, Dhanapal, & Balange, 2017), with unfrozen samples showing increased α-helices and β-turns but decreased β-sheets and random coils with more MTGase ($P < 0.05$), suggesting structural changes in MPs due to covalent cross-linking. F-T cycles led to a notable decrease in α-helices, with a shift towards β-sheets in uncross-linked MPs ($P < 0.05$). Leelapongwattana, Benjakul, Visessanguan, and Howell (2005) attributed the α-helix reduction to the loss of MPs structural integrity during freezing, contributing to gel degradation. Moreover, the transformed β-sheet structures were characterized by antiparallel intermolecular hydrogen bonding (non-naturally ordered structure), rather than naturally ordered structure, which were associated with protein cross-linking during freezing (Liang et al., 2020). MTGase treatment further diminished α-helix, β-sheet, and random coil structures in MPs sol, converting them to β-turns. This shift suggested that the combined effects of

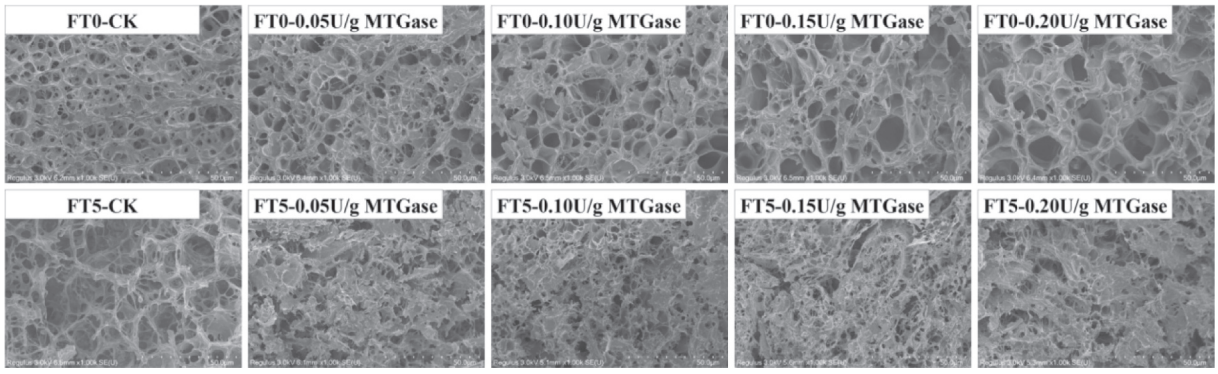

Fig. 3. Effects of MTGase on microstructure of gels prepared from unfrozen (FT 0) and freeze-thawed (FT 5) myofibrillar proteins (MPs) sols.

Table 3
Effects of MTGase on protein secondary structure of unfrozen (FT 0) and freeze-thawed (FT 5) myofibrillar proteins (MPs) sols.

	MTGase (U/g)	α-helix (%)	β-sheet (%)	β-turn (%)	Random coil (%)
FT 0	0	23.45 ± 0.08^{c}	27.53 ± 0.11^{b}	22.98 ± 0.06^{d}	26.04 ± 0.03^{a}
	0.10	24.06 ± 0.11^{b}	26.31 ± 0.30^{c}	24.08 ± 0.04^{c}	25.56 ± 0.23^{b}
	0.20	24.32 ± 0.06^{a}	25.80 ± 0.16^{d}	24.20 ± 0.01^{c}	25.69 ± 0.10^{b}
FT 5	0	23.05 ± 0.08^{d}	28.62 ± 0.12^{a}	22.54 ± 0.08^{e}	25.79 ± 0.11^{b}
	0.10	17.61 ± 0.03^{e}	23.58 ± 0.24 ^{e}	40.86 ± 0.19^{a}	17.96 ± 0.08^{c}
	0.20	17.73 ± 0.04^{e}	23.61 ± 0.12 ^{e}	40.62 ± 0.04^{b}	18.05 ± 0.03^{c}

Data are presented as mean ± SD (n = 3). Mean values in the same column with different.
Letters were significantly different ($P < 0.05$).

Table 4
Effects of MTGase on chemical bonds of unfrozen (FT 0) and freeze-thawed (FT 5) myofibrillar proteins (MPs) sols.

	MTGase (U/g)	Nonspecific bond (mg/mL)	Ionic bond (mg/mL)	Hydrogen bond (mg/mL)	Hydrophobic interaction (mg/mL)
FT 0	0	0.50 ± 0.01^{d}	5.07 ± 0.12^{a}	1.74 ± 0.04^{c}	2.45 ± 0.08^{d}
	0.10	0.45 ± 0.01^{e}	4.56 ± 0.16^{b}	2.15 ± 0.13^{b}	2.31 ± 0.15^{d}
	0.20	0.43 ± 0.01^{e}	3.70 ± 0.07^{c}	2.94 ± 0.19^{a}	2.19 ± 0.12^{d}
FT 5	0	1.09 ± 0.02^{a}	0.97 ± 0.02^{d}	0.88 ± 0.10^{d}	7.85 ± 0.16^{a}
	0.10	0.91 ± 0.02^{b}	0.54 ± 0.07^{e}	0.69 ± 0.05^{d}	6.51 ± 0.19^{b}
	0.20	0.83 ± 0.03^{c}	0.28 ± 0.05^{f}	0.72 ± 0.04^{d}	3.64 ± 0.18^{c}

Data are presented as mean ± SD (n = 3). Mean values in the same column with different.
Letters were significantly different ($P < 0.05$).

freezing and MTGase promoted protein unfolding, exposing reactive sites and facilitating further cross-linking in MPs sol (Yang et al., 2021). Notably, the decrease in α-helix content might impair the hydration between sol-state MPs and water, increasing water loss during gelation (Liang et al., 2020). Unlike heat-induced unfolding, the recrystallization and growth of ice crystals during F-T cycles might be responsible for the increased disordered structure (β-turn) in MTGase-catalyzed MPs sol (Zhuang et al., 2018).

3.4.2. Chemical bonds

Table 4 shows the impact of cross-linking on the molecular forces in MPs sols throughout F-T cycles. Predominantly, ionic bonds predominated in natural salt-extracted MPs sols, followed by hydrophobic and hydrogen bonds, with minimal non-specific interactions. Notably, disulfide bonds were nearly absent across all conditions (data not shown). After F-T cycles, an evident increase in nonspecific and hydrophobic interactions was observed compared to unfrozen sols ($P < 0.05$), but a significant reduction in ionic and hydrogen bonds ($P < 0.05$), indicating hydrophobic interactions as the main force driving protein cross-linking during freezing (Du et al., 2023). Typically, hydrophobic residues are concealed within the protein internal structures but become exposed in MPs sol due to salt-induced unfolding and ice crystal formation (An et al., 2018; Tong et al., 2023). The reduction in ionic and hydrogen bonds suggested protein denaturation and aggregation, potentially due to molecular rearrangement (Núñez-Flores, Cando, Borderías, & Moreno, 2018). This decrease notably compromised the water-holding capacity, as these bonds are crucial for protein-water interactions (Section 3.3.3). Furthermore, in cross-linked sols subjected to F-T cycles, all non-covalent interactions were diminished relative to non-cross-linked sols, implying that enzyme-induced non-disulfide covalent bonding disrupted the native MPs conformation and macromolecular gaps, thereby reducing non-covalent bonding (Xue et al., 2018).

3.4.3. Protein surface morphology

Surface morphologies of MPs aggregates treated with varying MTGase concentrations before and after F-T cycles were analyzed using AFM, presented in both two-dimensional (Fig. 4A-C) and three-dimensional (Fig. 4a-c) visuals. Unlike the dense aggregation observed in heat-induced gel, MPs sol featured a range of protein assemblies from monomers to polymers, characterized by discontinuous aggregation indicative of unstable protein cross-linking. Across all treatments, the aggregates displayed disordered globular structures characterized by "spongy fibrils", marked by dense fibrous networks and minor pores (indicated by arrows). The analysis revealed that the unfrozen control group exhibited smaller aggregates (protein height = 25.8 nm) and lower surface roughness (Rq = 3.37). In contrast, the aggregates in 0.1–0.2 U/g MTGase treatments were larger (protein height = 30.2–32 nm) with Rq values between 3.95 and 3.97, indicating enzyme-dependent formation of larger, irregular clusters of aggregates, corroborating particle size findings (Fig. S3). These large aggregates in sol were considered precursors to gel formation (Yang, Wang, & Chen, 2017). After F-T cycles, the control sample showed increased aggregation (protein height = 31.3 nm, Rq = 4.03), indicating further protein aggregation during frozen storage. Zhao, Liu, Hu, Li, and Li (2017) explained that proteins might be depolymerized by freezing and then tend to aggregate more substantially through new molecular interactions or self-folding. Conversely, the aggregate height decreased to

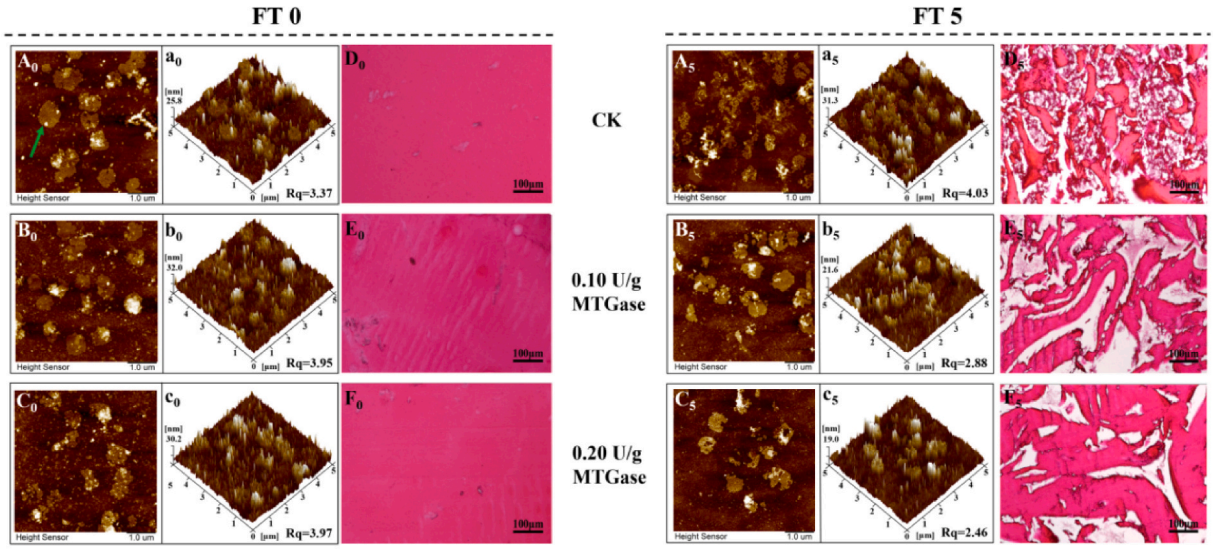

Fig. 4. Effects of MTGase on AFM images and microstructure of unfrozen (FT 0) and freeze-thawed (FT 5) myofibrillar proteins (MPs) sols. A_0-C_0: two-dimensional images of unfrozen sols; a_0-c_0: three-dimensional images of unfrozen sols; D_0-F_0: Microscope images of unfrozen sols; A_5-C_5: two-dimensional images of freeze–thawed sols; a_5-c_5: three-dimensional images of freeze-thawed sols; D_5-F_5: Microscope images of freeze-thawed sols. Data are presented as mean ± SD (n = 3).

21.6 and 19.0 nm, and Rq decreased to 2.88 and 2.46 as the samples with addition of 0.1–0.2 U/g MTGase, respectively. However, Dynamic Light Scattering (DLS) data indicated an increase in particle size after F-T cycles in MTGase-treated sols (Fig. S3), suggesting a discrepancy that could be due to the formation of large, insoluble aggregates not captured by AFM, similar to observations by Zhu, Zhang, Lin, and Tang (2017).

3.4.4. Sol microstructure

Microscopic analysis revealed the effects of F-T cycles and enzymatic treatment on MPs sol microstructure before thermal gelation, as shown in Fig. 4D-F. Initially, all unfrozen MPs sols displayed uniform and smooth microstructures without noticeable differences. However, the sol microstructures underwent varying degrees of aggregation and disruption after F-T cycles, and this destructive variation depends on the amount of MTGase added, aligning with the changes in gel microstructures (Section 3.3.4). Temperature fluctuations during F-T cycles facilitated ice crystal growth through recrystallization, disrupting the integrity of sol structure and the orderliness of subsequent heat-induced gel network. Liu et al. (2019) highlighted that ice crystals could damage protein structures during cold storage, leading to hydrophobic group exposure, protein denaturation, and polymerization, thereby creating larger pores and irregular networks. Our findings confirmed the transition of surimi from a sol to a weak gel state at low temperatures, driven by protein cross-linking and aggregation. This transformation, especially evident during F-T cycles, led to larger aggregates and structural gaps, adversely affecting the water retention capacity of MPs sols.

3.5. Correlation analysis

Correlation analysis revealed the effects of protein cross-linking on physicochemical properties of MPs sol during F-T cycles and heat-induced MPs gel after freezing (Fig. S4a, b). As expected, the degree of MTGase-catalyzed cross-linking, a critical variable, was significantly positively correlated with the hardness, springiness, and cooking loss of MPs gel ($P < 0.05$). Notably, weak cross-linking during freezing facilitated water migration and ice crystal formation, while MTGase further reduced bound water (T_{21a}, T_{21b}) stability in MPs sol. After five F-T cycles, the protein cross-linking degree, gel texture, and water retention positively correlated with α-helices, β-sheets, and random coils in sol-state MPs molecules, but negatively with β-turns ($P < 0.05$). Additionally, regardless of F-T cycles, gel texture and water-holding properties were significantly associated with nonspecific bonds, ionic bonds, hydrogen bonds and hydrophobic interactions in MPs sol ($P < 0.05$). These findings suggest that cross-linking treatment before freezing might modify MPs sol and gel states under F-T cycles by changing the molecular conformation and chemical interactions of MPs. Furthermore, compared to Fig. S4(a), Fig. S4(b) shows a stronger correlation between protein cross-linking degree and factors such as gel texture, moisture distribution, and cooking loss, indicating that the impact of protein cross-linking on the sol-gel transition in frozen surimi was more pronounced than in unfrozen surimi.

4. Conclusion

F-T cycles could mechanically damage MPs sol structure due to ice crystal formation, affecting moisture migration and textural properties. The cross-linking treatment with MTGase before freezing altered the molecular status and spatial conformation of sol-state MPs during F-T cycles, affecting the sol-gel transition after freezing. After five F-T cycles, heat-induced gels of cross-linked MPs sols exhibited more contracted microstructures, higher hardness, and springiness compared to the control group, due to higher protein aggregation from covalent cross-links, indicating that appropriate cross-linking degree before freezing can mitigate gel texture deterioration after freezing. However, after five F-T cycles, the cross-linked MPs sols showed fewer non-covalent interactions compared to the non-cross-linked group, impacting the binding of proteins with water. Consequently, this enhanced the mobility of bound water (T_{21a} and T_{21b}) within MPs sols, as well as the cooking loss in subsequent MPs gels. Correlation analysis indicated that changes in secondary structure and chemical forces in cross-linked MPs sols during F-T cycles were closely linked to the texture and water retention properties of subsequent thermal gels. An increase in β-turns positively affected gel hardness and springiness, while a decrease in other secondary structures (α-helices, β-sheets, and random coils) and non-covalent interactions (nonspecific bonds, ionic bonds, hydrogen bonds and hydrophobic interactions) was detrimental to gel water-holding capacity. This research deepens the understanding of the mechanism for controlling the quality of frozen surimi by regulating the protein molecule state before freezing.

CRediT authorship contribution statement

Yuxin Ding: Writing – original draft, Software, Methodology, Investigation, Formal analysis. **Ruonan Feng:** Software, Methodology, Formal analysis. **Zhifei Zhu:** Supervision, Resources. **Junmin Xu:** Visualization, Resources. **Yanshun Xu:** Writing – review & editing, Supervision, Resources, Funding acquisition, Conceptualization.

Declaration of competing interest

The authors declare that they have no known competing financial interests or personal relationships that could have appeared to influence the work reported in this paper.

Data availability

Data will be made available on request.

Acknowledgements

This work was supported by National Natural Science Foundation of China (NSFC 32172274); the earmarked fund for CARS (CARS-45-28), and the program of the "Collaborative innovation center of food safety and quality control in Jiangsu Province."

Appendix A. Supplementary data

Supplementary data to this article can be found online at https://doi.org/10.1016/j.fochx.2024.101448.

References

An, Y. Q., You, J., Xiong, S. B., & Yin, T. (2018). Short-term frozen storage enhances cross-linking that was induced by transglutaminase in surimi gels from silver carp (*Hypophthalmichthys molitrix*). *Food Chemistry, 257*, 216–222. https://doi.org/10.1016/j.foodchem.2018.02.140

Cao, M. J., Wang, J., Cao, A. L., Shiuan, D., Guan, R. F., Cai, L. Y., & Wang, Y. B. (2018). The impact of recrystallisation on the freeze-thaw cycles of red seabream (*Pagrus major*) fillets. *International Journal of Food Science & Technology, 54*(5), 1642–1650. https://doi.org/10.1111/ijfs.14039

Cao, Y., Zhao, L. Y., Huang, Q. L., Xiong, S. B., Yin, T., & Liu, Z. Y. (2022). Water migration, ice crystal formation, and freeze-thaw stability of silver carp surimi as affected by inulin under different additive amounts and polymerization degrees. *Food Hydrocolloids, 124*, Article 107267. https://doi.org/10.1016/j.foodhyd.2021.107267

Chen, X., Li, X. Z., Yang, F. J., Wu, J. H., Huang, D., Huang, J. L., & Wang, S. Y. (2022). Effects and mechanism of antifreeze peptides from silver carp scales on the freeze-thaw stability of frozen surimi. *Food Chemistry, 396*, Article 133717. https://doi.org/10.1016/j.foodchem.2022.133717

Chen, Z. H., Dai, Z. C., Liu, C. H., Wang, S., Li, J., & Mao, X. Z. (2024). Microbial transglutaminase promotes cross-linking for enhancing gelation of myofibrillar protein in frozen *Litopenaeus vannamei* through deamination reaction. *Food Hydrocolloids, 147*, Article 109332. https://doi.org/10.1016/j.foodhyd.2023.109332

Du, Z. Y., Yan, S. J., Feng, R. N., Li, J., Yu, D. W., Xia, W. S., & Xu, Y. S. (2023). Gel properties of refrigerated silver carp surimi sol as affected by cold-induced sol-gel transition and shearing. *LWT- Food Science and Technology, 190*, Article 115579. https://doi.org/10.1016/j.lwt.2023.115579

Fan, Y. T., Peng, G. F., Pang, X., Wen, Z., & Yi, J. (2021). Physicochemical, emulsifying, and interfacial properties of different whey protein aggregates obtained by thermal treatment. *LWT - Food Science and Technology, 149*, Article 111904. https://doi.org/10.1016/j.lwt.2021.111904

Fang, M. X., Luo, X. Y., Xiong, S. B., Yin, T., Hu, Y., Liu, R., … You, J. (2021). In vitro trypsin digestion and identification of possible cross-linking sites induced by transglutaminase (TGase) of silver carp (*Hypophthalmichthys molitrix*) surimi gels with different degrees of cross-linking. *Food Chemistry, 364*, Article 130443. https://doi.org/10.1016/j.foodchem.2021.130443

Feng, R. N., Li, J., Liu, C. K., Xia, W. S., & Xu, Y. S. (2022). Effects of actomyosin dissociation on the physicochemical and gelling properties of silver carp myofibrillar protein sol during freeze-thaw cycles. *Food Research International, 162*, Article 112075. https://doi.org/10.1016/j.foodres.2022.112075

Guo, X. J., Shi, L., Xiong, S. B., Hu, Y., You, J., Huang, Q. L., & Yin, T. (2019). Gelling properties of vacuum-freeze dried surimi powder as influenced by heating method and microbial transglutaminase. *LWT - Food Science and Technology, 99*, 105–111. https://doi.org/10.1016/j.lwt.2018.09.050

Huang, J. J., Bakry, A. M., Zeng, S. W., Xiong, S. B., Yin, T., You, J., … Huang, Q. L. (2019). Effect of phosphates on gelling characteristics and water mobility of myofibrillar protein from grass carp (*Ctenopharyngodon idellus*). *Food Chemistry, 272*, 84–92. https://doi.org/10.1016/j.foodchem.2018.08.028

Jia, D., Huang, Q. L., & Xiong, S. B. (2016). Chemical interactions and gel properties of black carp actomyosin affected by MTGase and their relationships. *Food Chemistry, 196*, 1180–1187. https://doi.org/10.1016/j.foodchem.2015.10.030

Leelapongwattana, K., Benjakul, S., Visessanguan, W., & Howell, N. K. (2005). Physicochemical and biochemical changes during frozen storage of minced flesh of lizardfish (*Saurida micropectoralis*). *Food Chemistry, 90*(1), 141–150. https://doi.org/10.1016/j.foodchem.2004.03.038

Liang, F., Lin, L., He, T. H., Zhou, X. H., Jiang, S. T., & Lu, J. F. (2020). Effect of transglutaminase on gel properties of surimi and precocious Chinese mitten crab (*Eriocheir sinensis*) meat. *Food Hydrocolloids, 98*, Article 105261. https://doi.org/10.1016/j.foodhyd.2019.105261

Liu, R., Zhao, S. M., Xie, B. J., & Xiong, S. B. (2011). Contribution of protein conformation and intermolecular bonds to fish and pork gelation properties. *Food Hydrocolloids, 25*(5), 898–906. https://doi.org/10.1016/j.foodhyd.2010.08.016

Liu, X. Y., Zhang, T., Xue, Y., & Xue, C. H. (2019). Changes of structural and physical properties of semi-gel from Alaska Pollock surimi during 4 °C storage. *Food Hydrocolloids, 87*, 772–782. https://doi.org/10.1016/j.foodhyd.2018.09.011

Liu, Y. T., Yang, X. X., Chi, Y. J., & Chi, Y. (2023). Effects of $CaCl_2$ on the rheology, microstructure and protein structures of rapidly salted separated egg yolk. *Food Research International, 172*, Article 113096. https://doi.org/10.1016/j.foodres.2023.113096

Luo, X. Y., Huang, K., Niu, Y. X., Zhang, X., An, Y. Q., Liu, R., … Hu, Y. (2024). Effects of freezing methods on physicochemical properties, protein/fat oxidation and odor characteristics of surimi gels with different cross-linking degrees. *Food Chemistry, 432*(30), Article 137268. https://doi.org/10.1016/j.foodchem.2023.137268

Nakazawa, N., & Okazaki, E. (2020). Recent research on factors influencing the quality of frozen seafood. *Fisheries Science, 86*(2), 231–244. https://doi.org/10.1007/s12562-020-01402-8

Núñez-Flores, R., Cando, D., Borderías, A. J., & Moreno, H. M. (2018). Importance of salt and temperature in myosin polymerization during surimi gelation. *Food Chemistry, 239*(15), 1226–1234. https://doi.org/10.1016/j.foodchem.2017.07.028

Pereira, J., Sathuvan, M., Lorenzo, J. M., Boateng, E. F., Brohi, S. A., & Zhang, W. (2021). Insight into the effects of coconut kernel fiber on the functional and microstructural properties of myofibrillar protein gel system. *LWT- Food Science and Technology, 138*, Article 110745. https://doi.org/10.1016/j.lwt.2020.110745

Priyadarshini, B., Xavier, K. A. M., Nayak, B. B., Dhanapal, K., & Balange, A. K. (2017). Instrumental quality attributes of single washed surimi gels of tilapia: Effect of different washing media. *LWT - Food Science and Technology, 86*, 385–392. https://doi.org/10.1016/j.lwt.2017.08.022

Sakamoto, H., Kumazawa, Y., Toiguchi, S., Seguro, K., Soeda, T., & Motoki, M. (2010). Gel strength enhancement by addition of microbial transglutaminase during onshore surimi manufacture. *Journal of Food Science, 60*(2), 300–304. https://doi.org/10.1111/j.1365-2621.1995.tb05660.x

Shao, J. H., Deng, Y. M., Song, L., Batur, A., Jia, N., & Liu, D. Y. (2016). Investigation the effects of protein hydration states on the mobility water and fat in meat batters by LF-NMR technique. *LWT - Food Science and Technology, 66*, 1–6. https://doi.org/10.1016/j.lwt.2015.10.008

Singh, A., Prabowo, F. F., Benjakul, S., Pranoto, Y., & Chantakun, K. (2020). Combined effect of microbial transglutaminase and ethanolic coconut husk extract on the gel properties and in-vitro digestibility of spotted golden goatfish (*Parupeneus heptacanthus*) surimi gel. *Food Hydrocolloids, 109*, Article 106107. https://doi.org/10.1016/j.foodhyd.2020.106107

Tang, S. W., Feng, G. X., Cui, W. X., Gao, R. C., Bai, F., Wang, J. L., … Zeng, M. Y. (2019). Effect of α-tocopherol on the physicochemical properties of sturgeon surimi during frozen storage. *Molecules, 24*(4), 710. https://doi.org/10.3390/molecules24040710

Tian, J., Walayat, N., Ding, Y. T., & Liu, J. H. (2021). The role of trifunctional cryoprotectants in the frozen storage of aquatic foods: Recent developments and future recommendations. *Comprehensive Reviews in Food Science and Food Safety, 21*(1), 321–339. https://doi.org/10.1111/1541-4337.12865

Tong, J. J., Jia, R., Xia, G. R., Zhang, X. X., Zhang, S. T., Wei, H. M., & Yang, W. G. (2023). Influence mechanisms of different setting time at low temperature on the gel quality and protein structure of *Solenocera crassicornis* surimi. *Food Bioscience, 51*, Article 102344. https://doi.org/10.1016/j.fbio.2022.102344

Wang, D. H., Zhou, F., Lai, D. N., Zhang, Y., Hu, J. M., & Lin, S. L. (2021). Curcumin-mediated sono/photodynamic treatment preserved the quality of shrimp surimi and influenced its microbial community changes during refrigerated storage. *Ultrasonics Sonochemistry, 78*, Article 105715. https://doi.org/10.1016/j.ultsonch.2021.105715

Wei, X. R., Monahan, F., Zhang, C. J., Wang, Z. Y., & Zhang, D. (2023). Exposure of hydrophobic groups affected the thermal aggregation of myosin based on experimental and molecular dynamics simulation. *LWT- Food Science and Technology, 187*, Article 115315. https://doi.org/10.1016/j.lwt.2023.115315

Xue, S. W., Xu, X. L., Shan, H. M., Wang, H. H., Yang, J., & Zhou, G. H. (2018). Effects of high-intensity ultrasound, high-pressure processing, and high-pressure homogenization on the physicochemical and functional properties of myofibrillar proteins. *Innovative Food Science & Emerging Technologies, 45*, 354–360. https://doi.org/10.1016/j.ifset.2017.12.007

Yang, C., Wang, Y. X., & Chen, L. Y. (2017). Fabrication, characterization and controlled release properties of oat protein gels with percolating structure induced by cold gelation. *Food Hydrocolloids, 62*, 21–34. https://doi.org/10.1016/j.foodhyd.2016.07.023

Yang, H. H., Zhong, C., Sun, L. C., Li, Y. K., Chen, H., & Wu, G. P. (2021). Effects of partial substitution of NaCl on myofibrillar protein properties from pearl mussel *Hyriopsis*

cumingii muscle: Structural characteristics and aggregation behaviors. *Food Chemistry, 356*, Article 129734. https://doi.org/10.1016/j.foodchem.2021.129734

Yang, N., Fan, X. R., Yu, W. Y., Huang, Y. Z., Yu, C. X., Konno, K., & Dong, X. P. (2020). Effects of microbial transglutaminase on gel formation of frozen-stored longtail southern cod (*Patagonotothen ramsayi*) mince. *LWT- Food Science and Technology, 128*, Article 109444. https://doi.org/10.1016/j.lwt.2020.109444

Zhang, B., Cao, H. J., Wei, W. Y., & Ying, X. G. (2020). Influence of temperature fluctuations on growth and recrystallization of ice crystals in frozen peeled shrimp (*Litopenaeus vannamei*) pre-soaked with carrageenan oligosaccharide and xylooligosaccharide. *Food Chemistry, 306*, Article 125641. https://doi.org/10.1016/j.foodchem.2019.125641

Zhang, N. N., Yang, N., Yu, W. Y., Jin, Z., Jiang, P. F., Yu, C. X., & Dong, X. P. (2021). Effects of microbial transglutaminase on textural, water distribution and microstructure of frozen-stored longtail southern cod (*Patagonotothen ramsayi*) fish mince gel. *Journal of Texture Studies, 53*(6), 1–10. https://doi.org/10.1111/jtxs.12657

Zhang, S., Meenu, M., Xiao, T., Hu, L. H., Ren, J. D., Ramaswamy, H. S., & Yu, Y. (2024). Insight into the mechanism of pressure shift freezing on water mobility, microstructure, and rheological properties of grass carp surimi gel. *Innovative Food Science & Emerging Technologies, 91*, Article 103528. https://doi.org/10.1016/j.ifset.2023.103528

Zhao, L., Liu, X. X., Hu, Z. Y., Li, L., & Li, B. (2017). Molecular structure evaluation of wheat gluten during frozen storage. *Food Biophysics, 12*, 60–68. https://doi.org/10.1007/s11483-016-9463-2

Zhou, Y., Liu, J. J. H., Kang, Y., Cui, H., & Yang, H. (2021). Effects of acid and alkaline treatments on physicochemical and rheological properties of tilapia surimi prepared by pH shift method during cold storage. *Food Research International, 145*, Article 110424. https://doi.org/10.1016/j.foodres.2021.110424

Zhu, X. F., Zhang, N., Lin, W. F., & Tang, C. H. (2017). Freeze-thaw stability of Pickering emulsions stabilized by soy and whey protein particles. *Food Hydrocolloids, 69*, 173–184. https://doi.org/10.1016/j.foodhyd.2017.02.001

Zhuang, X. B., Han, M. Y., Bai, Y., Liu, Y. F., Xing, L. J., Xu, X. L., & Zhou, G. H. (2018). Insight into the mechanism of myofibrillar protein gel improved by insoluble dietary fiber. *Food Hydrocolloids, 74*, 219–226. https://doi.org/10.1016/j.foodhyd.2017.08.015